SP Science Press

ARTICLE

Effect of Graphene Quantum Dots Addition on Microstructure and Properties of Supercritical Nanocomposite Coatings

Li Zhixian[1], Lei Weining[1,2], Li Yahan[1], Qian Haifeng[1], Mou Zhigang[3], He Bin[1]

[1] *School of Mechanical Engineering, Jiangsu University of Technology, Changzhou 213001, China;* [2] *Jiangsu Province Key Laboratory of Advanced Material Design and Additive Manufacturing, Changzhou 213001, China;* [3] *School of Chemistry and Chemical Engineering, Jiangsu University of Technology, Changzhou 213001, China*

Abstract: With graphene quantum dots (GQDs) of unique properties as the secondary phase additive, Ni-based nanocomposite coatings were prepared by supercritical electrodeposition technique. The effect of the addition of GQDs on the microstructure, microhardness, wear resistance, and corrosion resistance of the coatings under supercritical conditions was studied. Results show that the densification and homogenization occur in the coating microstructure after GQD addition. When the GQD content is 1.5 g/L, the surface morphology of the coating is more compact. X-ray diffraction analysis shows that the GQD addition can change the peak positions of (111), (200), and (222) nickel diffraction planes of the composite coatings, and the crystallographic preferred orientation appears in the (111) plane. The GQD addition greatly improves the properties of composite coatings. When the GQD content is 1.5 g/L, the coating microhardness is as high as 7381.4 MPa, which is nearly 980 MPa higher than that of the pure nickel coating. The cross-section area of the wear scar is 3336 μm^2, which is only 44% of that of the pure nickel coating. Tafel polarization test shows that the corrosion current density is 3.55×10^{-6} A·cm^{-2}, which is 65% lower than that of the pure nickel coating (10.07×10^{-6} A·cm^{-2}). The immersion corrosion tests of 150 h show that when the GQD content is 1.5 g/L, the optimal corrosion resistance occurs with the least pitting corrosion in the composite coating.

Key words: supercritical electrodeposition; graphene quantum dots; microstructure

In recent years, nickel plating and nickel electrodeposition have been widely used in industrial production due to the high hardness, excellent corrosion resistance, high wear resistance, and decorative properties of the coatings[1]. Nanocomposite coatings are usually covered on the surface of engineering materials by electrodeposition, which can effectively reduce the friction and wear of parts in the working environment, and enhance the wear resistance, friction reduction, and corrosion resistance of materials[2].

Graphene quantum dots (GQDs), a new type of zero-dimensional carbon-based nanomaterials, are graphene sheets with size of less than 100 nm[3–5]. Compared with the one/two-dimensional graphene sheets, GQDs have more obvious quantum confinement effects and sideband effects due to their small size, thereby leading to novel physicochemical properties[6], such as low biological toxicity, excellent water solubility, chemical inertness, stable photoluminescence, and good surface modification[7]. However, when GQD composite materials are prepared by thermal processing, such as electric spark sintering[8] and laser sintering[9], the special structure of GQDs will be damaged. Electrodeposition can enhance the properties of composite materials while retaining the structure of GQDs.

Through the suitable system temperature, pressure, and surfactant[10], the electrodeposition liquid can form excellent emulsification system during the electrodeposition, which involves the supercritical fluid and has excellent mass transfer performance. Therefore, the secondary phase additives[11–12] are effectively dispersed, the grains of the electrodeposited layer are refined, and the surface quality is greatly improved[13].

In this research, Ni-based composite coatings with GQD addition were prepared by supercritical electrodeposition technique. The effect of GQD content on microstructure, mechanical properties, and corrosion resistance of composite coatings was investigated to provide guidance for the development of metal matrix composite coatings. The preparation parameters used in this research for optimal coating are as follows: the current density is 6 A/dm^2, the pressure is 10 MPa, the temperature is 50 °C, and the plating time is 60 min.

1 Experiment

The schematic diagram of supercritical electroplating device is shown in Fig. 1. The pneumatic pump, cooling system, temperature measurement device, and temperature control device were used for supercritical electrodeposition. In this research, the anode and cathode were red copper plate of 20 mm×20 mm and pure nickel plate (purity of 99.9%) of 25 mm×25 mm, respectively. The distance between the two poles was 20 mm. The red copper plate was descaled, degreased, deoxidized, ground, and polished; the pure nickel plate was descaled, degreased, and deoxidized. The pre-treated plates were fixed on the anode and cathode electrode plates with insulating glue. Polyethylene glycol trimethyl nonyl ether (TMN, $C_{12}H_{26}O \cdot (C_2H_4O)_n$) surfactant was added to the electroplating solution, and GQDs were fully dispersed. The solution was stirred before electroplating by Chunlin ultrasonic cleaner and EMS-12 split magnetic stirrer. The related process parameters and added GQD content of nickel coating (Ni) and different supercritical GQD composite coatings (Ni-GQDs-I, Ni-GQDs-II, Ni-GQDs-III) are shown in Table 1, and the composition of electroplating solution is listed in Table 2.

The prepared GQD composite coatings and the Ni coating were characterized by EFI Tecnai G2 F20 transmission electron microscope (TEM). The state of GQDs in the composite coatings was observed by high-resolution transmis-sion electron microscope (HRTEM), and the elements of the composite coatings were analyzed by energy dispersive spectrometer (EDS). Sigma-500 scanning electron microscope (SEM) was also used to observe the morphology of the coatings before and after immersion corrosion. X'PERT POWDER X-ray diffractometer (XRD, Cu-Kα radiation) was used to analyze the preferred orientation of nickel crystals in the coatings. The scanning range was 10°–80° and the step size was 0.013 130 3°. HXD-1000TMS/LCD digital micro-hardness tester was used to test the coating hardness. Each specimen was tested at 5 different points, and the average hardness was used for analysis. Nanovea TRB friction and wear test machine was used to test the wear resistance of the coatings. The steel ball with diameter of 6 mm was selected as the friction pair, the rotation speed was 200 r/min, the load was 10 N, and the test time was 15 min. Nanovea PS50 optical profiler was used to observe the surface topography of the wear scar. The scan area was 2 mm×2 mm, the step size was 10 μm, and the scan rate was 3.33 mm/s. CHI760E electrochemical workstation was used to test the Nyquist spectrum and Tafel polarization curve of the coatings. The coatings were immersed in 3.5wt% NaCl solution at room temperature and ambient pressure for 150 h, then rinsed with alcohol, and finally observed by SEM.

2 Results and Discussion

2.1 Effect of GQD content on coating microstructure

2.1.1 Effect of GQD content on surface morphology of coating

Fig. 2a and 2b show TEM microstructures of the Ni-GQDs-II composite coating. Fig. 2c shows the selected area electron diffraction (SAED) pattern of Ni-GQDs-II composite coating. It can be seen that the GQDs are evenly distributed in the coating surface and are closely combined with the nickel grains. According to Fig. 2b, the rhombic lattice can be clearly observed, which represents the typical multilayer graphene, indicating that GQDs are tightly bound with the nickel grains. The diffraction ring in Fig. 2c is a polycrystalline diffraction ring, including (111), (200), and (222) crystal planes, which shows that the Ni crystal structure in the composite coating is a face-centered cubic structure. It can be seen from Fig. 2d that the content of nickel and carbon elements at point A is 94.47wt% and 5.52wt%, or 77.75at% and 22.24at%, respectively. It is suggested that carbon element exists in the composite coating, i.e., GQDs are embedded in the composite coating.

Fig. 3 shows SEM surface morphologies of Ni coating and

Fig.1   Schematic diagram of supercritical electrodeposition device with CO_2 fluid

Table 1   Preparation process parameters of nickel coating and different supercritical GQD composite coatings

Specimen	Current density/A·dm^{-2}	Pressure/MPa	Temperature/°C	Electroplating duration/min	GQD concentration/g·L^{-1}
Ni-GQDs-I	6	10	50	60	1.0
Ni-GQDs-II	6	10	50	60	1.5
Ni-GQDs-III	6	10	50	60	2.0
Ni	6	10	50	60	0

Table 2   Composition of electroplating solution

Composition	Concentration/g·L^{-1}
$NiSO_4·6H_2O$	300.0
$NiCl_2·6H_2O$	30.0
H_3BO_3	35.0
$C_{12}H_{25}NaO_4S$	0.2
TMN surfactant	0.15

GQD composite coatings with different GQD contents under supercritical condition. As shown in Fig. 3a, the surface density of Ni coating is not high and the particle size distribution is uneven. After adding GQDs, the particle distribution of GQD composite coating is uniform, the surface density is high, and the coating shows better sphericity. Particularly, the Ni-GQDs-II composite coating has a more uniform particle size distribution and a higher surface density. This is because the addition of GQDs provides nucleation sites for the reduced nickel atoms on the cathode surface, thus preventing the growth of metallic nickel. Therefore, the metallic nickel is uniformly dispersed and deposited on the cathode surface, resulting in the high surface density and better sphericity of the coating. However, with further increasing the GQD content, GQDs cannot be completely dispersed, leading to the agglomeration. The agglomerated GQDs can hardly enter the coating. Even though they could, their agglomerated state would result in the coarser grains of composite coating. Therefore, the Ni-GQDs-II composite coating has high surface density, uniform particle size distribution, and better sphericity, compared with other

coatings. The GQD addition in Ni-GQDs-I composite coating is insufficient, whereas that in Ni-GQDs-III composite coating is excess. The addition of 1.5 g/L GQD is optimal.

2.1.2   Preferential orientation of nickel crystals in coatings under different preparation conditions

Fig. 4 shows XRD patterns of Ni coating and GQD composite coatings with different GQD contents. The diffraction peaks of all coatings are similar, and the corresponding crystal planes are (111), (200), and (220) planes[14]. It can be seen that the Ni crystal structure is a face-centered cubic structure, which is consistent with the results of SAED pattern. Besides, compared with that of the Ni coating, the diffraction intensity of (111) and (200) planes is decreased in the GQD composite coatings. The diffraction intensity of the (200) plane decreases significantly, and that of the (222) plane increases slightly. The GQD composite coatings show a preferred orientation on the (111) plane. It indicates that the addition of GQDs has an effect on the nickel crystallization and changes the process of nickel nucleation and growth during electrodeposition. According to the diffraction peak width and the Scherrer formula, the coating grain size D can be obtained, as follows:

$$D = \frac{K\gamma}{B\cos\theta} \tag{1}$$

where K is Scherrer constant; γ is the X-ray wavelength; B is the half-height width of the diffraction peak; θ is Bragg diffraction angle. K is 0.89 and γ is 0.154 056[15–17]. The obtained coating grain size is shown in Table 3. It is found that the grain sizes of the GQD composite coatings are smaller than that of the Ni coating. Among the GQD composite
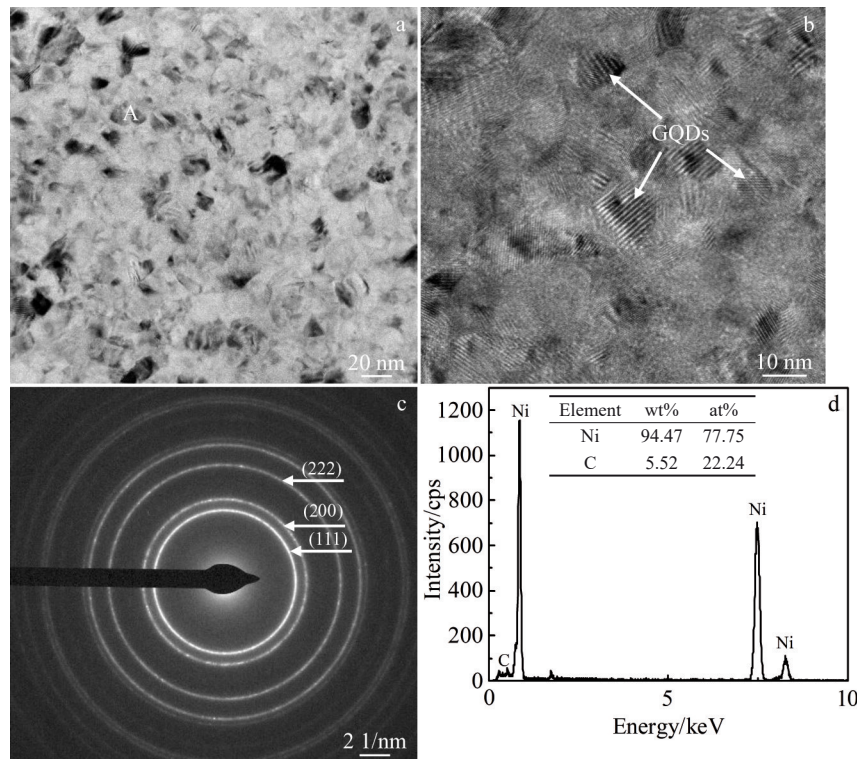
Fig.2   TEM microstructures (a, b) and SAED pattern (c) of Ni-GQDs-II composite coating; EDS analysis results of point A in Fig.2a (d)
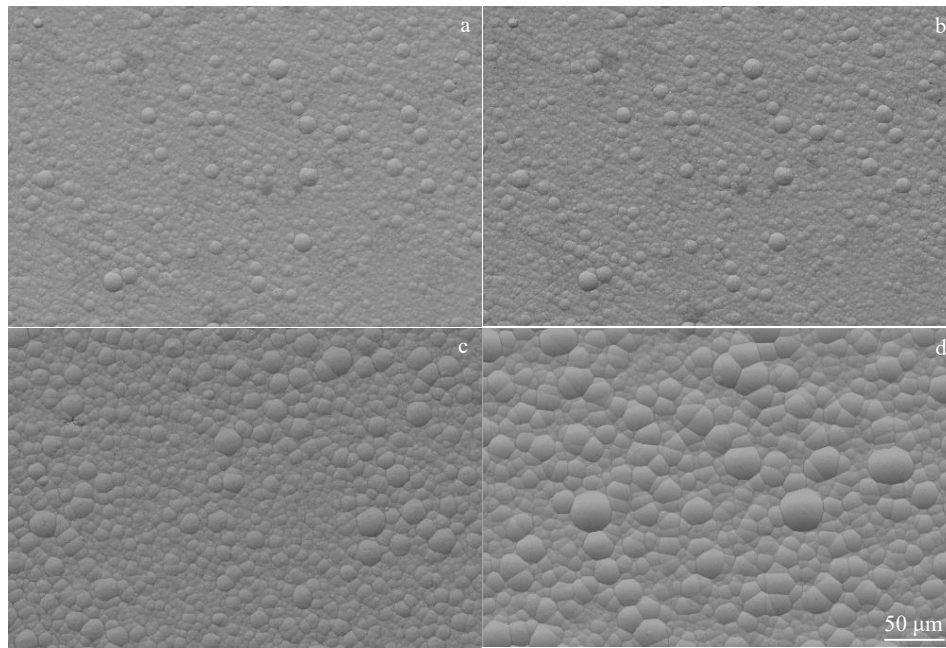
Fig.3   SEM surface morphologies of Ni coating (a), Ni-GQDs-I coating (b), Ni-GQDs-II coating (c), and Ni-GQDs-III coating (d)
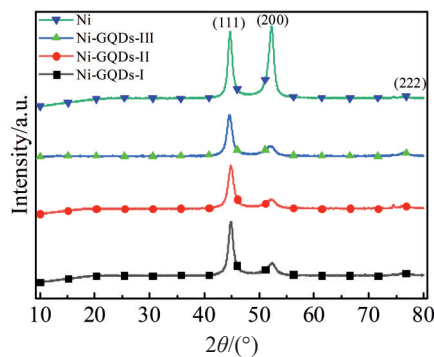
Fig.4   XRD patterns of Ni coating and different GQD composite coatings

Table 3   Grain sizes of Ni coating and different GQD composite coatings

Specimen	Grain size, D/nm
Ni-GQDs-I	31.5
Ni-GQDs-II	26.6
Ni-GQDs-III	28.4
Ni	36.2

coatings, the grain size of Ni-GQDs-II composite coating is the smallest. It can be concluded that an appropriate amount of GQD addition positively affects the mass transfer process of matrix metal deposition during the electrodeposition. In the process of metal nucleation, the addition of GQDs provides nucleation points and restricts the continuous growth of nickel atoms, thereby refining the coating grains and reducing the grain size.

2.2   Effect of GQD content on coating properties

2.2.1   Effect of GQD content on microhardness

As shown in Fig. 5, the microhardness of Ni coating is the lowest. With increasing the GQD content, the microhardness of GQD composite coating is increased firstly and then decreased. When GQD content is 1.5 g/L, the microhardness $HV_{0.2}$ of composite coating reaches 7381.4 MPa, which is nearly 980 MPa higher than that of Ni coating. This is because the absorption capacity of cations in the electroplating solution is enhanced after GQDs are added into the electroplating solution. With increasing the GQD content in the plating solution, the GQDs cause more crystal planes on the metal crystal surface, which provides more nickel-ion nucleation points. Thus, the nucleation is promoted and the grain growth is hindered, resulting in denser coating and refined grains. When GQDs are excessively added, the GQDs cannot be sufficiently dispersed, leading to the agglomeration. Therefore, the Ni-GQDs-II composite coating has the highest microhardness.
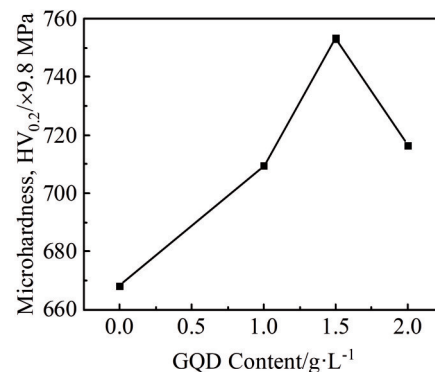
Fig.5   Microhardness of different GQD composite coatings

2.2.2 Effect of GQD content on wear resistance

Fig.6 and Fig.7 show the 3D images and the cross-sections of the wear scars of the Ni coating and GQD composite coatings, respectively. Table 4 shows the maximum depths, cross-section areas, and volume wears of the wear scars of the Ni coating and GQD composite coatings. It can be seen that the maximum depths of wear scar of the GQD composite coatings are less than that of the Ni coating. With increasing the GQD content, the maximum depth of wear scar is gradually decreased. The cross-section areas and volume wears of wear scar of the GQD composite coatings are smaller than those of the Ni coating. Among the GQD composite coatings, the Ni-GQDs-II composite coating has the smallest cross-section areas and volume wear of wear scar. The cross-section area of wear scar of the Ni-GQDs-II composite coating is 50.2%, 92.0%, and only 44% of that of the Ni-GQDs-I composite coating, Ni-GQDs-II composite coating, and Ni coating, respectively. Compared with the Ni coating, the GQD composite coatings have better wear resistance due to the local adhesion and shear of GQDs in the connection area. The GQD composite coatings have larger contact areas when the transverse shear force occurs due to their fine grains and relatively smooth surface. The Ni-GQDs-II composite coating has finer grain, smoother surface, and denser internal,
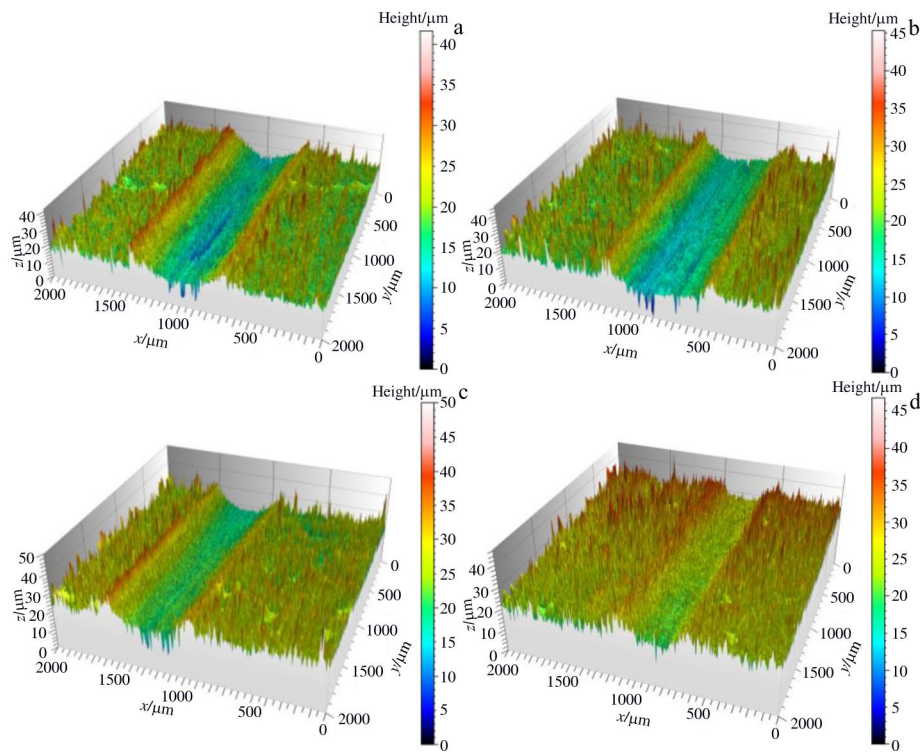
Fig.6   3D images of wear scar of Ni coating (a), Ni-GQDs-I coating (b), Ni-GQDs-II coating (c), and Ni-GQDs-III coating (d)
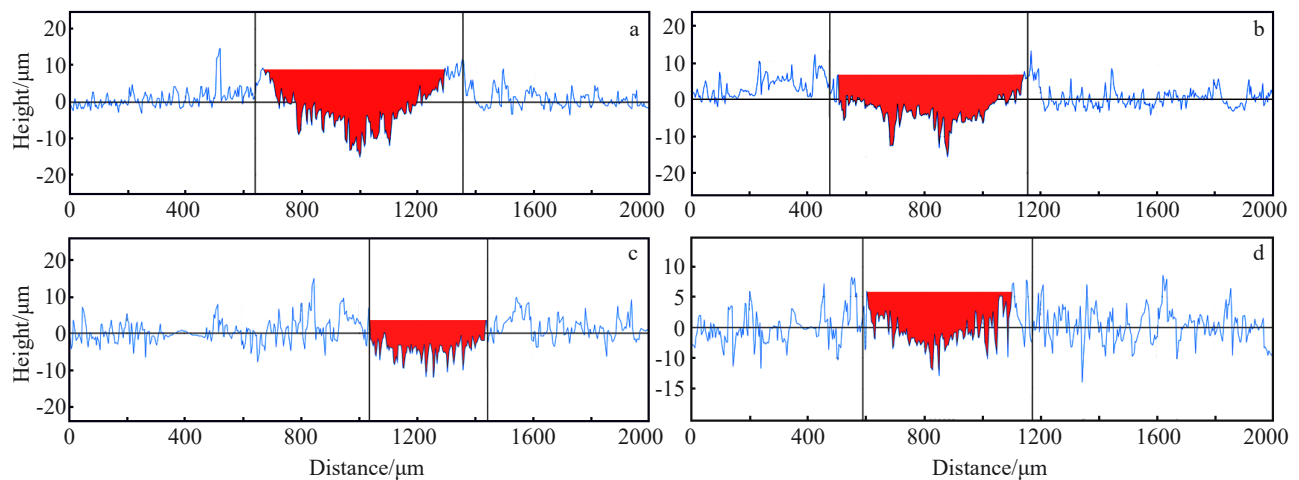
Fig.7   Cross-sections of wear scar of Ni coating (a), Ni-GQDs-I coating (b), Ni-GQDs-II coating (c), and Ni-GQDs-III coating (d)

Table 4 Maximum depth, cross-section area, and volume wear of wear scar in Ni coating and different GQD composite coatings

Specimen	Maximum depth/μm	Cross-section area/μm^2	Volume wear/ ×10^{-7} μm^3
Ni-GQDs-I	22.5	6644	6.644
Ni-GQDs-II	17.0	3336	3.336
Ni-GQDs-III	12.2	3626	3.626
Ni	24.2	7546	7.546

structure. Therefore, the Ni-GQDs-II composite coating has better wear resistance, and the wear resistance of the GQD composite coatings is better than that of the Ni coating, which is consistent with the results of microhardness.

2.2.3 Effect of GQD content on corrosion resistance

Fig. 8 shows the Nyquist plots, Tafel polarization curves, and Bode plots of the Ni coating and GQD composite coatings in 3.5wt% NaCl solution. It can be seen that the capacity arc radius of different coatings is ordered as follows: Ni＜Ni-GQDs-III＜Ni-GQDs-I＜Ni-GQDs-II. After GQD addition, the impedance of the coatings is increased. When GQD content is 1.5 g/L, the coating resistance reaches the maximum, i. e., the corrosion resistance of Ni-GQDs-II composite coating is optimal. When GQD content is 2.0 g/L,

the coating resistance is decreased, indicating that the corrosion resistance of Ni-GQDs-III composite coating deteriorates. From the Tafel polarization curves and the Tafel fitting results in Table 5, it can be seen that the corrosion potential and corrosion current density of the Ni-GQDs-II composite coating are −376 eV and 3.55×10^{-6} A·cm^{-2}, respectively. Compared with other coatings, its corrosion potential is the highest; its corrosion current density is the lowest, which is 65% lower than that of the Ni coating. It can be concluded that the Ni-GQDs-II composite coating exhibits excellent corrosion resistance. Compared with the Ni coating, the Ni-GQD composite coatings have relatively high self-corrosion potential and relatively low corrosion current density, which indicates that the corrosion resistance of GQD composite coatings is better than that of the Ni coating. According to Fig. 8c, both the GQD composite coatings and the Ni coating have only one phase angle peak, which is consistent with the single capacitive arc of each coating in Fig. 8a. As shown in Fig. 8d, the capacitive modulus of the Ni-GQDs-II composite coating is larger than that of other GQD composite coatings, which further proves that the Ni-GQDs-II composite coating has better corrosion resistance. The fitting circuit analysis of the Nyquist and Bode plots was conducted by ZSimpWin software, and the schematic diagram of equivalent circuit model is shown in Fig. 9, where R_1 is the resistance of the
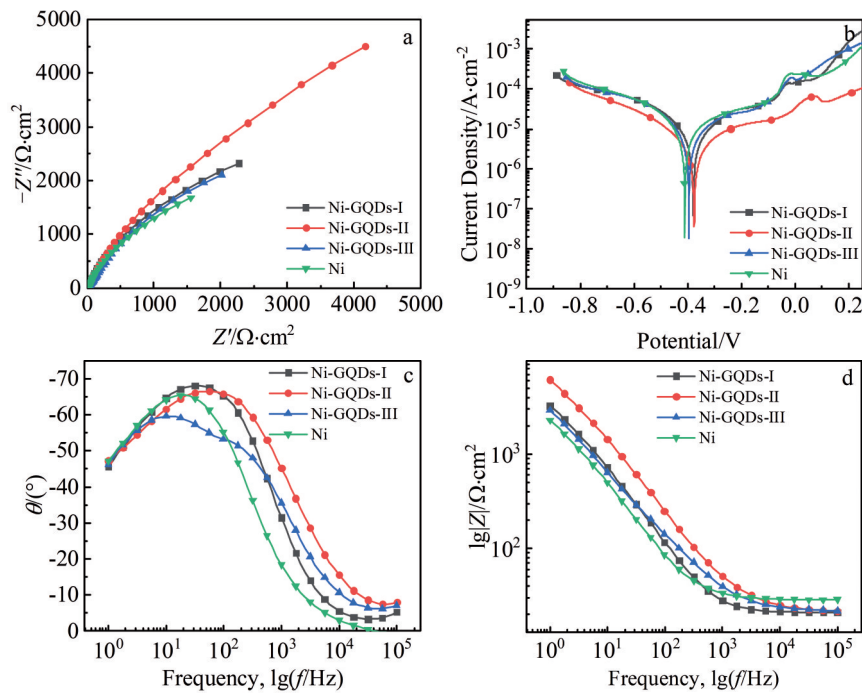
Fig.8 Nyquist plots (a), Tafel polarization curves (b) and Bode plots (c, d) of Ni coating and different GQD composite coatings

Table 5 Tafel fitting results of Ni coating and different GQD composite coatings

Specimen	Corrosion potential, E_{corr}/eV	Corrosion current density, I_{corr}/×10^{-6} A·cm^{-2}
Ni-GQDs-I	−379	6.60
Ni-GQDs-II	−376	3.55
Ni-GQDs-III	−395	7.61
Ni	−410	10.07
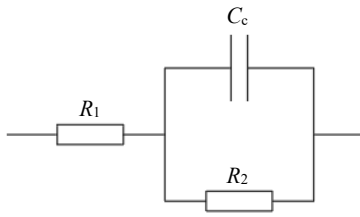
Fig.9　Schematic diagram of equivalent circuit model

Table 6　Fitting results of equivalent circuit for Ni coating and different GQD composite coatings ($\Omega \cdot cm^2$)

Specimen	R_1	R_2
Ni-GQDs-I	92.41	12 600
Ni-GQDs-II	114.00	22 470
Ni-GQDs-III	118.40	10 350
Ni	127.50	9 147

plating solution, C_c is the capacitance of the coating, and R_2 is the resistance of the coating. The fitting results are shown in Table 6. The resistance of the GQD composite coatings is greater than that of the Ni coating, and with increasing the GQD content, the resistance is increased firstly and then decreased.

After the GQD addition, GQDs act as a barrier to prevent the corrosive substances. After the GQDs are evenly distributed in the coating, the GQDs superimposed layer by layer can form a protective film to reduce the infiltration of corrosive substances, such as chloride ions and oxygen, and inhibit the cathodic reaction to a certain extent, thus reducing the cathodic reaction rate. When GQD addition is insufficient, the generated protective film is relatively weak, and the infiltration of corrosive substances can easily occur. However, the excess addition of GQDs causes the uneven dispersion, thus leading to the agglomeration and rare entrance into the coating. Thus, the protective film is weak or unevenly strong,
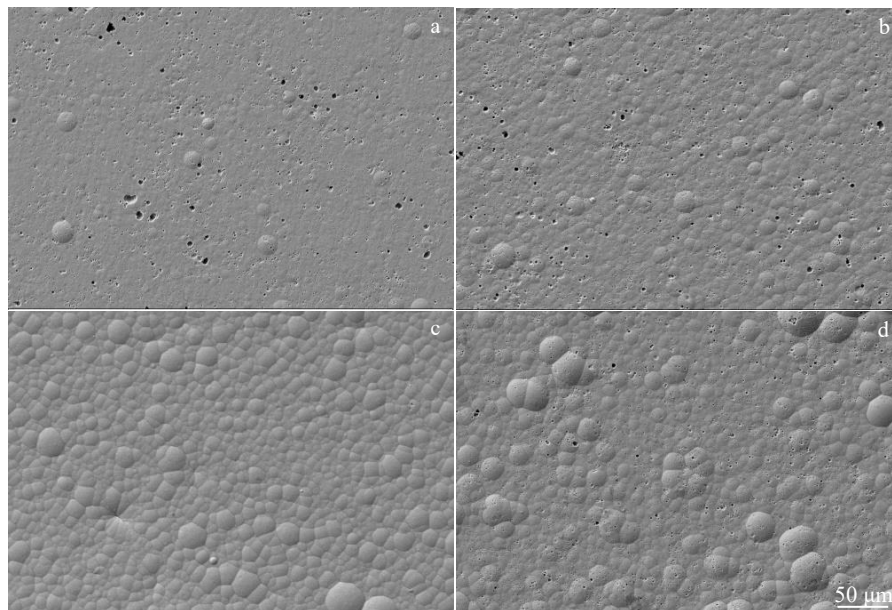
Fig.10　SEM surface morphologies of Ni coating (a), Ni-GQDs-I coating (b), Ni-GQDs-II coating (c), and Ni-GQDs-III coating (d) after immersion in 3.5wt% NaCl solution at room temperature for 150 h

resulting in the easy corrosion by corrosive substances. Therefore, the Ni-GQDs-II composite coating shows the optimal corrosion resistance.

Fig.10 shows SEM surface morphologies of the Ni coating and GQD composite coatings after immersion in 3.5wt% NaCl solution at room temperature for 150 h. Under the erosion of Cl⁻ and other corrosive substances, only the Ni-GQDs-II composite coating does not show obvious pitting corrosion. Compared with those of the Ni-GQDs-I and Ni-GQDs-III composite coatings, the corrosion pits of the Ni coating are deeper and larger, i. e., the pitting corrosion of the Ni coating is more serious. In general, the Ni-GQDs-II composite coating exhibits excellent corrosion resistance.

3　Conclusions

1) The graphene quantum dots (GQDs) are evenly distributed in the composite coating surface and are closely combined with the nickel grains in the Ni-based composite coating after GQD addition. When GQDs are used as the secondary phase additive for electrodeposition, the grains can be refined and the coating presents better sphericity. When GQD content is 1.5 g/L, the GQDs in the composite coating are more uniformly dispersed, resulting in denser coating surface.

2) The addition of GQDs changes the preferred orientation of the coating grains. The grain size is reduced, and the coating grains are refined.

3) The microhardness of the Ni-based composite coating

with GQD content of 1.5 g/L is nearly 980 MPa higher than that of the Ni coating, and it is the highest among the GQD composite coatings. The cross-section area and volume wear of wear scar of composite coating with GQD content of 1.5 g/L are the smallest, indicating that this composite coating is superior in microhardness and wear resistance.

4) The composite coating with GQD content of 1.5 g/L has the smallest corrosion rate and corrosion tendency, presenting excellent corrosion resistance. Nearly no pitting corrosion occurs in the composite coating with GQD content of 1.5 g/L, further proving its excellent corrosion resistance.

References

1　Long Qiong, Lu Fanghai, Luo Xun *et al. Hydrometallurgy of China*[J], 2018, 37(3): 179 (in Chinese)

2　Zhang Xiaoyu, Xia Tiandong, Xu Yangtao *et al. Metallic Functional Materials*[J], 2015, 22(4): 51 (in Chinese)

3　Wang Shuhong, Zhang Huanping, Du Hui *et al. Applied Chemical Industry*[J], 2015, 44(4): 732 (in Chinese)

4　Asmaa K A, Zulkarnain Z, Araa M H *et al. The Journal of Physics and Chemistry of Solids*[J], 2021, 153: 110 006

5　Zhou Y, Sun Z P, Yu Y *et al. Tribology International*[J], 2021, 159: 106 933

6　Diao Yuqi, Li Tiening. *Chinese Journal of Power Sources*[J], 2017, 41(8): 1229 (in Chinese)

7　Cheng Chaoge, Li Min, Wu Qinlin. *Journal of Functional Materials*[J], 2017, 48(4): 4033 (in Chinese)

8　Bochenek D. *Materials*[J], 2022, 15(7): 2524

9　Schubert O, Edelhoff D, Erdelt K *et al. International Journal of Computerized Dentistry*[J], 2022, 25(2): 151

10　Chuang H C, Jiang G W, Sanchez J. *Ultrasonics Sonochemistry*[J], 2020, 60: 104 805

11　Hou Zhenchang, Nie Zhihua, Liu Zhichao *et al. Journal of Alloys and Compounds*[J], 2021, 865: 158 872

12　Ejaz N, Ali L, Mansoor M. *Key Engineering Materials*[J], 2021, 875: 302

13　Zhang Hongzhuang, Li Changyou, Yao Guo *et al. International Journal of Fatigue*[J], 2022, 160: 106 838

14　Xu Juliang, Chen Tingshui. *Physical Testing and Chemical Analysis Part A: Physical Testing*[J], 2016, 52(3): 164 (in Chinese)

15　Sumadiyasa M, Manuaba I B S. *Buletin Fisika*[J], 2018, 19(1): 28

16　Hall B D, Zanchet D, Ugarte D. *Journal of Applied Crystallography*[J], 2000, 33(6): 1335

17　Patterson A L. *Physical Review*[J], 1936, 56(10): 978

石墨烯量子点添加量对超临界纳米复合镀层微观结构与性能影响

李志贤[1]，雷卫宁[1,2]，李雅寒[1]，钱海峰[1]，牟志刚[3]，何　斌[1]

(1. 江苏理工学院 机械工程学院，江苏 常州 213001)

(2. 江苏省先进材料设计与增材制造重点实验室，江苏 常州 213001)

(3. 江苏理工学院 化学化工学院，江苏 常州 213001)

摘　要：以性能独特的石墨烯量子点（GQDs）为第二相添加物，采用超临界电沉积技术制备 Ni 基纳米复合镀层，研究超临界条件下 GQDs 添加量对镀层的微观结构、显微硬度、耐磨性能、耐腐蚀性能等的影响。结果表明：加入 GQDs，镀层微观结构致密化和均匀化。当 GQDs 添加量为 1.5 g/L 时，镀层表面形貌更为致密。X 射线衍射分析显示，GQDs 的添加，改变了复合镀层镍衍射面（111）、（200）及（222）峰位，在（111）面产生结晶择优取向。GQDs 的添加大幅提升了复合镀层的各项性能。当 GQDs 添加量为 1.5 g/L 时，镀层显微硬度高达 7381.4 MPa，比纯镍镀层显微硬度高近 980 MPa；磨痕截面积为 3336 μm^2，仅为纯镍镀层的 44%。Tafel 极化试验结果表明，腐蚀电流密度为 3.55×10^{-6} A·cm^{-2}，相较于纯镍镀层的 10.07×10^{-6} A·cm^{-2}，降低了 65%；150 h 浸泡腐蚀实验表明，当 GQDs 添加量为 1.5 g/L 时，镀层点蚀最少，耐腐蚀性能最为优异。

关键词：超临界电沉积；石墨烯量子点；微观结构

作者简介：李志贤，男，1997年生，硕士生，江苏理工学院机械工程学院，江苏 常州 213001，E-mail：105731951@qq.com